

# CHROMATICALLY CORRECTED IMAGING SYSTEMS FOR CHARGED-PARTICLE RADIOGRAPHY\*

Barbara Blind<sup>#</sup> and Andrew J. Jason, LANL, Los Alamos, New Mexico, U.S.A.

## Abstract

In proton radiography, imaging with systems consisting of quadrupole magnets is an established technique for viewing the material distribution and composition of objects, either statically or during fast events such as explosions. With the standard magnet configuration, the  $-I$  lens, chromatic aberrations generally dominate the image blur. Image resolution can be improved, and largely decoupled from the input-beam parameters, by using a second-order achromat with some additional higher-order aberration correction. The aberration-correction approach is discussed. For a given resolution, such an achromat allows use of much lower-energy imaging particles than a  $-I$  lens. Each achromat design can be scaled into many equivalent systems; an 800-MeV proton design and its equivalent 40-MeV electron system are presented. The electron system is useful for imaging thin objects. Magnet errors in the achromats must be tightly controlled to preserve image quality, but not beyond feasibility of present technology. System performance is verified by particle tracking. Configurations alternative to the canonical achromat are discussed.

## RADIOGRAPHY OVERVIEW

The fundamentals of charged-particle radiography, by now well established, are discussed elsewhere [1]. A beam traverses an object and experiences path-dependent attenuation, multiple Coulomb scattering (MCS) and energy loss. The particles exiting the object are refocused onto an image plane. The standard configuration used is the  $-I$  lens, which has chromatic and geometric aberrations. The latter can be effectively corrected with octupoles if desired. With an input beam of the proper correlations, the effects of the chromatic aberrations are minimized and the beam is sorted by MCS angle at the center of the  $-I$  lens, the so-called Fourier point (FP). An aperture (collimator) at this location can discriminate against particles with a particular scattering history and can thus increase image contrast. Images of two  $-I$  lenses with appropriate collimators allow deduction of material distribution and composition (density, atomic number) of the object. Even with a chromatically matched input beam chromatic aberrations, mainly from terms linear in both MCS angle and momentum deviation, lead to image blur. This is mitigated by going to high-energy particles (e.g. protons of tens of GeV) or limiting oneself to thin objects [2,3]. Los Alamos radiographers and their collaborators have done extensive work using 800-MeV protons at the Los Alamos Neutron Science Center (LANSCE) and 23-

GeV protons at Brookhaven National Laboratory (BNL) and hence examples are for these two energies.

## ACHROMATIC LENS SYSTEMS

Chromatic-aberration correction requires a beamline with dispersion, generated by inclusion of dipole magnets, and multipole correctors in the dispersive regions.

A well-known such system is a second-order achromat with four or more identical cells containing dipoles and quadrupoles [4]. In the resulting  $+I$  lens, two families of sextupoles correct the second-order chromatic aberrations without causing second-order geometric aberrations. The sextupoles do cause third-order aberrations not present in a  $-I$  lens, but superior image resolution is typically noted for achromatic lenses at the same particle energy.

In theory, a third-order achromat can be designed by adding seven families of octupoles to the two families of sextupoles of a second-order achromat with five or more cells [5]. In practice, this results in a system in which the octupoles buck each other and have strong fields, with consequent large higher-order aberrations.

The designs presented here are second-order achromats with three families of octupoles to cancel some of the third-order aberrations. For compactness, the quadrupoles have sextupole and octupole components, so that only one dedicated octupole per cell is present.

For a fixed layout, the sextupole integrated strengths (and thus the third-order aberrations caused by the sextupoles) are essentially independent of magnet lengths. The sextupole integrated strengths can be adjusted by adjusting the dipole bend angle or the drift lengths. The quadrupole fringe fields generate third-order geometric aberrations proportional to their gradients, which can be adjusted by adjusting the magnet lengths. For achromats with five or more cells, a combined-function-quadrupole length can be chosen such that the two types of geometric aberrations largely cancel. Algorithms for minimizing residual aberrations have not yet been fully developed.

It is important to have the option of inserting FP apertures. Because there are no other restrictions on the input-beam correlations, they can be chosen for accessibility of the FP location and to minimize aperture requirements. There will be dispersion at the FP and this fact needs to be considered when choosing FP-aperture dimensions and in interpreting collimated images.

## THEORETICAL PERFORMANCE LIMITATIONS

Even absent all aberrations (i.e. for a perfect  $-I$  or  $+I$  lens) particles from a point inside an object do not fall on a single point at the image plane. A ray of particles traversing an object of thickness  $t$  experiences MCS and

\*Work supported by the US Department of Energy under contract W7405-ENG-36

<sup>#</sup>bblind@lanl.gov

emerges with a projected angular distribution with an rms of  $k\sqrt{t}$ , where  $k$  is a constant depending on object material and particle energy.

Assume that a point a distance  $a \cdot t$  ( $0 < a < 1$ ) upstream of the end of the object lies in the plane being imaged. From this point originate particles of various angles, each experiencing MCS through the remainder of the object. As viewed from downstream of the object, the beam originating from this point has an apparent rms size  $s$ , due to body blur, with

$$s^2 = \frac{1}{3} k^2 a^3 t^3.$$

For tungsten (W),  $k \approx 0.0187$  rad/ $\sqrt{\text{cm}}$  for 800-MeV protons and  $k \approx 0.00096$  rad/ $\sqrt{\text{cm}}$  for 23-GeV protons. Assuming that the angular acceptance of the lens is unlimited, a point at the center ( $a=0.5$ ) of a 40 g/cm<sup>2</sup> W plate ( $t=2$  cm) is imaged with  $s \approx 108$   $\mu\text{m}$  and  $s \approx 5.6$   $\mu\text{m}$ , respectively.

The dominant chromatic-aberration coefficients of  $-I$  lenses are  $T_{126}$  and  $T_{346}$ , with numerical values of about 0.1 mm/(mrad%) for an 800-MeV and 0.3 mm/(mrad%) for a 23-GeV system. Chromatic blur can be computed from the product of the coefficient, MCS angle, and beam momentum spread. Assuming a 2-cm range of thicknesses in a real object, the chromatic blur has an rms value of 6,200  $\mu\text{m}$  at 800 MeV and 50  $\mu\text{m}$  at 23 GeV.

Thus the chromatic blur overwhelms the body blur but their ratio decreases with increasing momentum. Both effects increase with object thickness as  $t^{3/2}$ . Collimation, either at the FP or by lens angular acceptance, decreases the blur from both effects, but decreases the body blur more strongly. A highly corrected (including magnet errors) achromat will allow the body blur to be approached as a fundamental limitation.

An achromat eliminates the effect of chromatic limbing, i.e., oscillations of the image intensity near an edge. The achromat curvature prevents secondary particles from the object from reaching the imaging detector.

## PERFORMANCE ASSESSMENT BY PARTICLE TRACKING

The performance of an imaging system must be acceptable over the area known as the field of view (FOV). The system must clear particles up to the desired MCS angle and must accommodate momentum deviations of a prescribed amount.

For a quick quality assessment of a particular design, test particles were launched from 121 equidistant points on the FOV. From each point originated 27 particles, with nominal and non-nominal divergences and momenta. This beam was tracked element by element with the third-order code MARYLIE [6].

To better study the performance of a system, a uniformly distributed beam was launched from the horizontal axis, sent through a simple object and then transported to the image plane. The object was a 2-cm-thick W plate with a 2-mm-wide 1-cm-deep vertical groove centered on the vertical axis. Depending on the

magnet settings of the imaging system, particles having traversed a particular thickness of W are in focus. At the image plane, profiles were generated from those particles within a narrow (0.2-mm-high) band around the horizontal axis. The edges of the groove must be discernible for the system to perform acceptably.

## CONCEPT OF EQUIVALENT SYSTEMS

The design and construction of a small achromat was considered that would be used for electron radiography of light objects and serve as a prototype for a large, more expensive 800-MeV achromat. An energy of 40 MeV was chosen for the electron system. Both systems were optimized in the same way.

In equivalent systems, all physical dimensions (longitudinal and transverse) of the small system are smaller than those of the large system by a factor of  $\xi$ , but the dipole bend angles are the same. The non-zero transfer-matrix elements between object and image plane scale in such a way that the test-beam scatter plots at the image planes of the two systems look identical when the input beam of the small system has spatial coordinates that are smaller by a factor of  $\xi$  than those of the large system, while the divergences and momentum deviations remain the same.

### 800-MeV Proton System

At the time of this design, the objective was to find an 800-MeV achromat small enough to fit into LANSCE Area C. Consequently, a five-cell system was chosen as a strawman design, with each cell containing the elements shown in Table 1. The layout is shown in Figure 1. For comparison, an 800-MeV  $-I$  lens is also shown.

Table 1: Elements of one cell of 800-MeV achromat.

element	length	description
drift	1.250 m	
multipole	0.500 m	+4.65 T/m, +2.20 T/m <sup>2</sup> , -1.25 T/m <sup>3</sup>
drift	0.445 m	
dipole	0.880 m	1.16 T, 12° angle, 0.2-m full gap
drift	0.445 m	
multipole	0.500 m	-4.47 T/m, -3.98 T/m <sup>2</sup> , -0.99 T/m <sup>3</sup>
drift	0.650 m	
octupole	0.200 m	+3.82 T/m <sup>3</sup>
drift	0.400 m	

A 10-cm by 10-cm FOV was desired. Thus, points from which test particles were launched were 1.0 cm apart. The chosen input-beam correlations produced a FP 1.0 m downstream of the end of the first cell and corresponded to near-minimum aperture requirements to clear the desired  $\pm 10$ -mrad MCS angles and  $\pm 5\%$  energy deviations (0.16-m quadrupole aperture radius and 0.2-m dipole full gap). In order to assess the beam-optics performance of

the system, the test particles were given divergence deviations of 0 mrad and  $\pm 10$  mrad to simulate MCS, and had momentum deviations of 0% and  $\pm 3.23\%$ . The test beam at the image plane is shown on the left-hand side of Figure 2. Without aberrations there would be 121 distinct points.

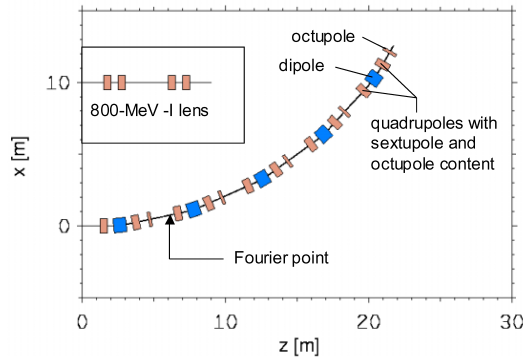


Figure 1: Layout of strawman five-cell 800-MeV proton achromat. The 800-MeV  $-I$  lens is shown for comparison.

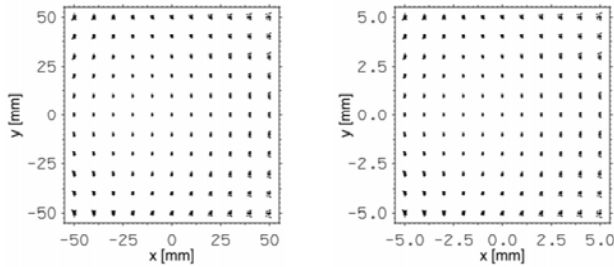


Figure 2: Test beams at image plane of 800-MeV proton achromat (left) and 40-MeV electron achromat (right).

### 40-MeV Electron System

All physical dimensions of the 40-MeV electron system are smaller by a factor of 10 than those shown in Table 1 for the proton system. The system has a 1.0-cm by 1.0-cm FOV and the input-beam correlations are larger by a factor of 10 than the input-beam correlations of the proton system, while the divergence and momentum deviations are the same. The test beam at the image plane is shown on the right-hand side of Figure 2. Except for the change in scale this scatter plot is indistinguishable from the scatter plot on the left-hand-side of Figure 2.

## PERFORMANCE COMPARISONS OF ACHROMATS AND $-I$ LENSES

### Using Test Particles

Test particles, launched from the object plane of the achromat of Table 1 and from the object plane of an 800-MeV  $-I$  lens with a 1.5-m standoff distance, were compared. Figure 3 shows the test particles originating on the axis (top) and at the lower left-hand corner (bottom) of the achromat (left) and the  $-I$  lens (right). Test particles had MCS angles of 0 mrad and  $\pm 10$  mrad and momentum deviations of 0.0% and  $\pm 3.23\%$ .

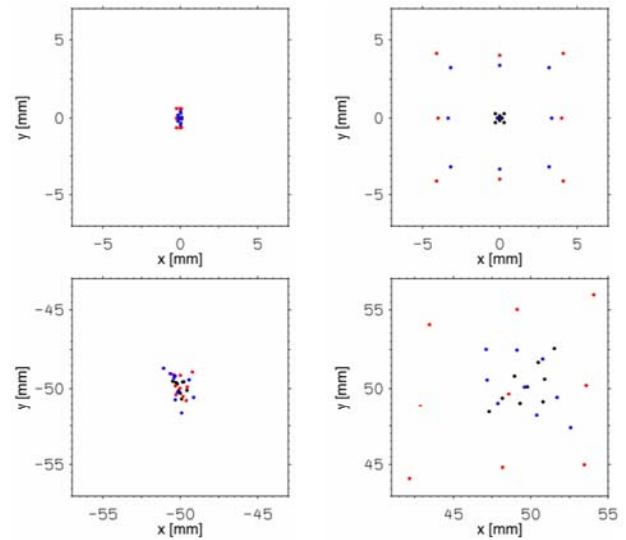


Figure 3: Test particles with momentum deviations of 0.0% (black), +3.23% (blue) and  $-3.23\%$  (red) at image plane of 800-MeV achromat (left) and  $-I$  lens (right).

The higher-order aberrations of the  $-I$  lens are evident from the fact that the blue and red dots do not coincide for the beam launched on axis. The high-order nature of the achromat is obvious from the irregular pattern of the beam at the image plane. The achromat clearly outperforms the  $-I$  lens despite residual third-order aberrations.

### By Tracking through the Simple Object

The simple object was studied with the 800-MeV achromat, 800-MeV  $-I$  lens, and 23-GeV BNL  $-I$  lens [7].

Figure 4 (top) shows the profiles at the image plane of the 800-MeV achromat with the system focused on an average particles energy, without (left) and with (right) a FP aperture. Figure 4 (bottom) shows the profiles with the system focused on particles having traversed the plate (left) or groove (right), both times with a collimator present. The elliptical FP apertures were dimensioned

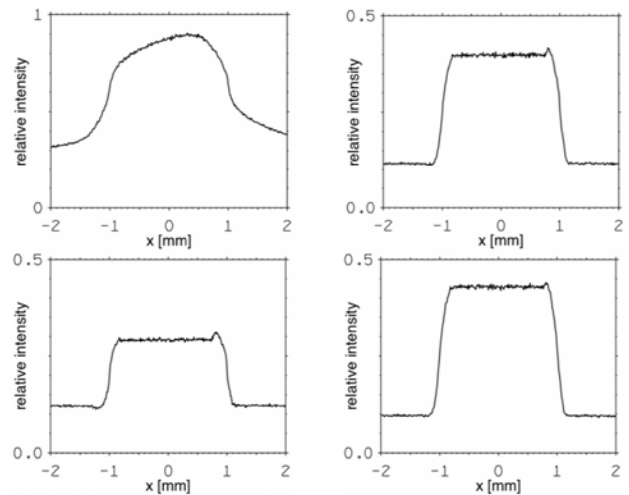


Figure 4: Intensity profiles of simple-object image, for 800-MeV achromats configured as described in text.

to pass a 10-mrad MCS angle and were centered on the portion of the beam with the smaller MCS angles (i.e. particles from the groove).

The system accepts MCS angles up to 10 mrad and thus not all protons exiting the object arrive at the FP. The collimator also removes a significant fraction of the beam. Therefore, the intensity profiles shown in Figure 4 for cases with FP apertures are magnified by a factor of two.

Figure 5 shows particle scatter plots at the image plane of the 800-MeV achromat for the configurations resulting in the profiles of Figure 4, bottom.

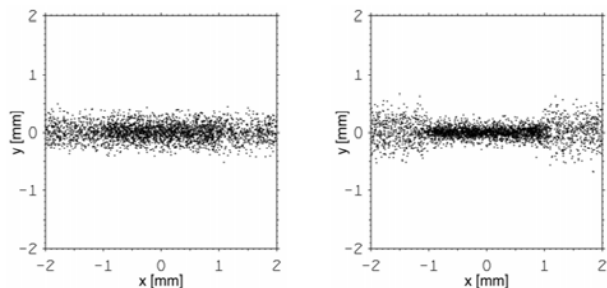


Figure 5: Scatter plots of beam at image plane, for simple object and 800-MeV achromat focused on particles having traversed plate (left) or groove (right).

It is common to use two  $-I$  lenses in series to allow repeated angle cuts to determine material properties. For an achromat, there is a second FP downstream of the one utilized above. In achromats with an even number of cells the second FP falls on an identical cell location as the first one, while for an achromat with an odd number of cells there is no common downstream location for the horizontal and vertical FP and the downstream FPs typically are in inaccessible locations. For this reason (absent space constraints) a six-cell achromat is preferable to a five-cell one. It also has a  $-I$  image, albeit in a region with dispersion, at the end of the third cell.

While in actuality it is not possible to utilize the downstream FPs of the five-cell achromat of Table 1, in simulations it is possible to place collimators at these locations. Figure 6 shows the profile at the image plane with the system focused on particles from the plate, with the upstream FP aperture and a second horizontal FP aperture, again centered on the beam from the groove. The profile is similar to the bottom-left profile of Figure 4, but with decreased intensity in the plate region.

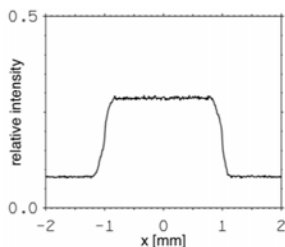


Figure 6: Intensity profile of simple-object image, for 800-MeV achromat focused on particles having traversed plate and containing two FP apertures.

Figure 7 shows the profiles at the image plane of the 800-MeV  $-I$  lens, with the system focused on particles from the plate (left) or groove (right). The round FP apertures, centered on axis, were dimensioned to pass a 10-mrad scattering angle. In order to better understand Figure 7, the corresponding scatter plots are given in Figure 8. With the system focused for particles having traversed the plate, the particles from the groove experience very large aberrations leading to an actual decrease in intensity in the groove region. With the system focused for particles having traversed the groove, the particles from the plate experience large aberrations. Neither focus produces an acceptable image.

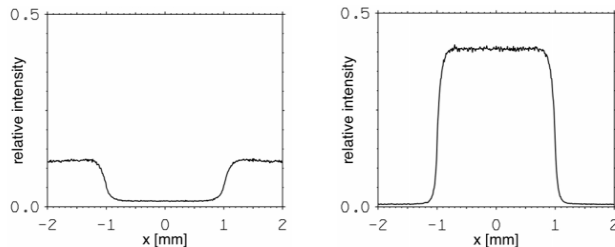


Figure 7: Intensity profiles of simple-object image, for 800-MeV  $-I$  lenses configured as described in text.

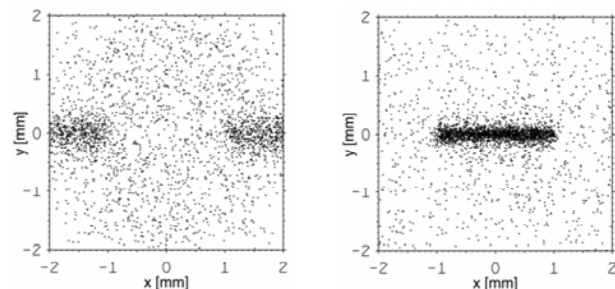


Figure 8: Scatter plots of beam at image plane, for simple object and 800-MeV  $-I$  lens focused on particles having traversed plate (left) or groove (right).

Figure 9 shows the profiles at the image plane of the 23-GeV BNL  $-I$  lens, with the system focused on particles from the plate (left) or groove (right). This system clearly outperforms the 800-MeV achromat, at the cost of a much larger beam energy. Small chromatic-imbining effects are seen in Figure 9.

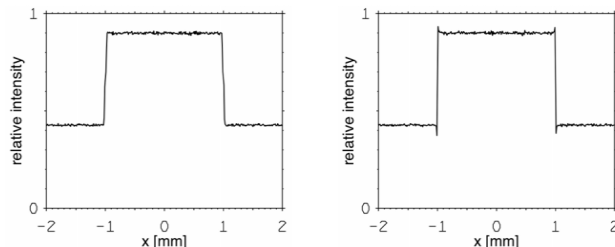


Figure 9: Intensity profiles of simple-object image, for 23-GeV BNL  $-I$  lenses configured as described in text.

## MAGNET ERRORS

An error-free achromatic lens clearly outperforms an error-free  $-I$  lens for particles of the same energy. On the other hand, an achromatic lens has many more magnetic elements than a  $-I$  lens and it needed to be shown that the performance of such a system is not compromised by magnet errors.

In order to establish error limits for the components of the achromat, an error study was performed that considered random and systematic dipole-field and quadrupole-gradient errors, random and systematic multipole content of dipoles and quadrupoles up to duodecapoles, and dipole, combined-function quadrupole and multipole misalignments. Both individual errors and combinations of errors were considered. Each case was studied by performing a set of runs simulating 10,000 different achromats with the error(s) in question. Errors were randomly chosen and uniformly distributed within given limits.

For the error study, the figure of merit was the average radius of three sets of 36 particles, each on a 10-mrad angle cone but with momentum deviations of  $-3.23\%$ ,  $0.0\%$  and  $+3.23\%$ , relative to a reference particle of nominal momentum and divergence. These particles were launched either on axis or from the upper right-hand corner of the FOV. For the error-free achromat the average radius, an indication of resolution, is  $270\ \mu\text{m}$  and  $517\ \mu\text{m}$ , respectively, at these two locations. Each set of runs resulted in a range of average radii.

Error limits were established from the requirement that no error type by itself may produce more than a  $50\ \mu\text{m}$  average-radius range. This lead to 50 distinct error limits for the 50 types of errors studied, some of them tight and others easy to achieve. In summary, field stability of  $10^{-4}$  is needed, along with multipole content of dipoles and quadrupoles not exceeding between  $2 \cdot 10^{-4}$  and  $10^{-3}$  of the main fields, at the aperture radius or dipole gap. For the lower harmonics, some adjustment of the multipole correctors is possible and the skew components might be remediable by extra (very weak) skew correctors. Quadrupole transverse alignment must be very tight, especially in the horizontal plane, while good dipole transverse alignment is not crucial. The yaw and pitch of neither matters, but the roll also needs to be tightly controlled. Both normal-conducting and superconducting magnets were considered. While error specifications are tight, they are achievable. Magnets can be superconducting for power and stability, but heating by particles outside the acceptance may quench magnets.

## ALTERNATIVE ACHROMAT CONFIGURATIONS

The achromat as described, with angle monotonically increasing along its length, is only one of a wide range of possible second-order achromats. Other configurations of interest are obtained by considering system symmetries, and second-order achromaticity can in general be qualified by inspection. A few examples are given in

Figure 10. In a) a four-cell monotonic bend is shown. In b) the configuration is modified to alternate bend directions. In c) and d) eight-cell configurations are shown that require less lateral space than would an extension of a). Configuration d) requires a total phase advance of  $4\pi$  while the others have  $2\pi$ . The first half of d) cannot be made into a first-order or second-order achromat. Other restrictions apply to further alterations of the configurations. However, any number of cells can be added to a). Reverse-bend cells are characterized by a sign change of even-order elements.

A second-order analytical thin-lens formalism for a FODO lattice with a dipole centered between quadrupoles established analytical insight into element strengths. Sextupole strengths are entirely determined by relations of the form  $q/L^2b$ , where  $q$  is a numerical constant dependent on sextupole family and configuration,  $L$  is half the cell length and  $b$  is the  $R_{16}$  matrix element of the thin-lens dipole. For the layouts considered, results are within a few percent of numerical thick-lens calculations. While the reverse-bend configurations may be more desirable for construction considerations, the alteration of symmetry causes substantially higher sextupole strengths with corresponding enhancement of third-order aberrations.

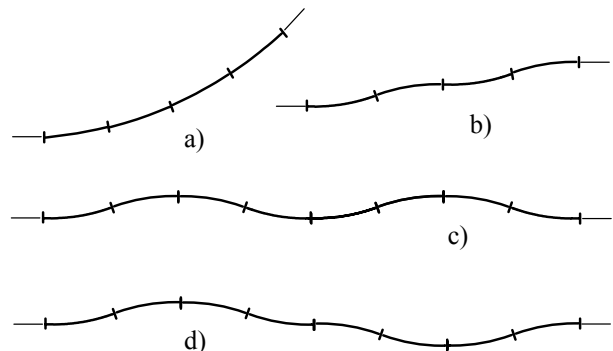


Figure 10: Sketches of selected second-order achromats.

## REFERENCES

- [1] C.T. Mottershead and J.D. Zumbro, "Magnetic Optics for Proton Radiography," PAC'97, Vancouver, B.C., Canada, p. 1397.
- [2] G.E. Hogan, et al., "Proton Radiography," PAC'99, New York, NY, USA, p. 579.
- [3] T. Mottershead, et al., Design and Operation of a Proton Microscope for Radiography at 800 MeV," PAC'03, Portland, OR, USA, p.702.
- [4] K.L. Brown, "A Second-Order Magnetic Optical Achromat," SLAC-PUB-2257, February 1979.
- [5] A.J. Dragt, et al., "MARYLIE Users' Manual," University of Maryland Department of Physics and Astronomy technical report, chapter 10.6.1.
- [6] A.J. Dragt, et al., "MARYLIE Users' Manual," University of Maryland Department of Physics and Astronomy technical report.
- [7] K.R. Alrick, et al., "Some Preliminary Results from Experiment 933," Los Alamos National Laboratory technical report, LA-UR-00-4796, September 2000.